Simulation of Micro-Channel Flows by Lattice Boltzmann Method

C. Y. Lim [1] and C. Shu[2]

Department of Mechanical Engineering, National University of Singapore

Abstract

In the present work, we extend the LBM (Lattice Boltzmann Method) to simulate the steady state, pressure driven micro-channel flows. LBM is a particle-based method, which is different from the conventional Navier-Stokes solvers where the continuum assumption is applied, and a slip boundary condition is implemented for the micro flow. Its mesoscopic representation of particle's kinetics is also much different to that used in direct numerical simulations such as DSMC (Direct Simulation of Monte Carlo). It is believed that LBM has a potential in simulating the micro flow. In this model, we pay particular attention in obtaining the pressure distribution of flow across the channel within the slip flow regime ($0.001 < Kn < 0.1$) with the consideration of rarefaction and minute dimension effects ($Kn = l/H$). We obtain favourable results that demonstrate the non-linearity and compressibility effect occurred in the pressure distribution of a micro-channel flow. We also manage to capture the desired slip phenomenon at the solid wall, which remains the major interest in micro-scaled flow simulation.

[1] Research Student, [2] Supervisor

Keywords: Lattice Boltzmann Method, Discrete Boltzmann Equation, Micro Flow, Rarefaction, Compressibility, and Slip.

I. Introduction

The existence of Micro-machining technology such as surface and bulk machining enables us to fabricate mechanical systems in micron size, which are generally referred as the micro-electro-mechanical systems, or MEMS. The advent of these micro-systems complements the development and understanding of new regimes in micro flow by making experimental work possible, which in turn help calibrating MEMS and understanding their characteristics like a feedback loop. The main incentive to look at fluidic behaviour at micron scale is that micro devices tend to behave much differently than the objects we are used to handling in daily life, requiring us to bring in more factors into consideration. The initial forces, e.g., tend to be quite small and the surface effects such as friction, electrostatic forces and viscous effects tend to dominate their overall behaviour as the surface to volume ratio becomes larger.

Minute dimensions have also extended these flow phenomena to higher degrees of rarefaction, which is often characterised by Knudsen number *Kn*, where *Kn* is the ratio of the mean free path $\boldsymbol{l}$ to the characteristic length *L*. It is generally agreed that continuum fluid flow holds until $Kn = 0.1$, beyond which the continuum assumption breaks down in rarefaction due to sharp gradients of the flow parameters. The major concern in applying Navier-Stokes equations beyond this regime is that there may be

simply too few molecules within a finite volume for continuum assumption to be valid. For this reason, the direct simulation of Monte Carlo (DSMC) [1] has become a popular method in simulating rarefied flows, especially in high attitude atmosphere. Although this physical approach has some advantages over the traditional N-S solvers, this molecular model is generally much more demanding of computing resources. Here we propose an extension of Lattice Boltzmann Method (LBM) based on a discrete Boltzmann equation approach [2-5] which is much computationally efficient than DSMC for simulating of micro flow. LBM has gained much attention in simulating fluid flow since 1980s for its efficient parallel computational algorithm. Somewhat different from DSMC in its mesoscopic representation of molecular kinetics, this method strictly involves 2 updating processes: local collision and streaming propagation. Paying particular attention to flow ranging $0.050 < Kn < 0.155$, we perform simulations for 2D pressure driven micro-channel flow and compare our results with analytical solutions based on N-S equations as well as experimental results in present work. Detailed numerical methodology will be given in the next section, which are subsequently followed by result discussions and concluding remarks.

II. Methodology

a. Discrete Boltzmann Equation

The origin of LBM can be traced back to the Lattice-Gas Cellular Automata (LGCA) [6], in which similar kinetic equation was shared:

$$f_i(\vec{x} + e_i\Delta\vec{x}, t + \Delta t) = f_i(\vec{x}, t) + \Omega_i(f_i(\vec{x}, t)) \qquad i=1,\ldots,k \qquad (1)$$

where f_i was the Boolean algebra indicating occupation state of particles in *i* direction and *k* was the total number of lattice links; the last term W_i in the equation represented the collision operator in accordance to arbitrary collision rules. Recent Lattice Boltzmann Models are further simplified by replacing the Boolean algebra with a continuous distribution function [5] and linearising the collision operator by BGK collision term [7-8], in which the non-linear term W_i is expressed as the single time relaxation of f_i to local equilibrium [9], yielding:

$$f_i(\vec{x} + e_i\Delta\vec{x}, t + \Delta t) = f_i(\vec{x}, t) - \frac{1}{t}\left[f_i(\vec{x}, t) - f_i^{eq}(\vec{x}, t)\right] \qquad i=0,1,\ldots,k \qquad (2)$$

where f_i^{eq} is the local equilibrium distribution function. Conventional approach is to apply Chapman-Enskog multi-scale expansion in recovering the N-S equations; here we take a different route by looking at Boltzmann equation, which is more applicable in simulating rarefied flow. We are only concerned about the degree of rarefaction in general, regardless of its density and dimension. Boltzmann equation involves velocity distribution function in velocity space:

$$\frac{\partial f(\vec{v})}{\partial t} + C\nabla f(\vec{v}) = Q \qquad (3)$$

where C is the stream molecular velocity and Q is the collision integral, which will be linearized by BGK collision term onwards. As we intend to solve the flow in x-y plane, we consider f as a function of $\vec{v}$, x, y and t:

$$\frac{\partial f(\vec{v},x,y,t)}{\partial t} + c\nabla f(\vec{v},x,y,t) = -\frac{1}{t}\left[f(\vec{v},x,y,t) - f^{eq}(\vec{v},x,y,t)\right] \tag{4}$$

This continuous function f can be further latticed by a finite set of velocities, as suggested by its name Lattice Boltzmann Model. As illustrated in Figure 1, we restrict these velocities into a few lattice vectors of unity components, namely c_i, where $i = 0, 1,\ldots, k$ where i denotes the lattice direction:

$$\frac{\partial f_i(x,y,t)}{\partial t} + c_i\nabla f_i(x,y,t) = -\frac{1}{\boldsymbol{t}}\left[f_i(x,y,t) - f_i^{eq}(x,y,t)\right]. \tag{5}$$

Non-dimensionalising Equation (5) by the characteristic length L, reference speed U, reference density n_r, and collision time t_c, we have $F_i = f_i / n_r$, $\hat{t} = t \cdot U / L$, $\hat{t} = t / t_c$ and $\hat{\nabla} = L\nabla$, giving the discrete Boltzmann form [10]:

$$\frac{\partial F_i(\hat{x},\hat{y},\hat{t})}{\partial \hat{t}} + c_i\nabla F_i(\hat{x},\hat{y},\hat{t}) = -\frac{1}{\hat{\boldsymbol{t}}\boldsymbol{e}}\left[F_i(\hat{x},\hat{y},\hat{t}) - f_i^{eq}(\hat{x},\hat{y},\hat{t})\right] \tag{6}$$

where the parameter $\boldsymbol{e}$ may be interpreted as the Knudsen number Kn, where the mean free path being $U^{\chi}\, t_c$ and the characteristic length being L. The stream velocity c_i can be

considered as the root mean square speed or the mean speed in a specific direction *i*, and in our lattice context, they are the lattice vectors of unity velocity components. We employ a square lattice multi-speed model, denoted by [11] D2Q9 for its historical reasons as below:

$$c_0 = (0,0)$$
$$c_i = \left(\cos\left(\frac{i-1}{4}\right)\pi, \sin\left(\frac{i-1}{4}\right)\pi\right)\cdot c \qquad i = 1,\ldots, 8 \qquad (7)$$

Multi-speed models were developed to account for unphysical flow effects such as Galilean invariance [12] and explicitly pressure-velocity dependence problem as discussed by Chen et al [13]. In the early development of LGCA and LBM, lattice tensor isotropy had to be satisfied up to the 4^{th} order in order to recover Navier-Stokes equations in macroscopic limit. Generally, a 'reasonable' lattice has to be invariant with respect to any arbitrary orthogonal transformations in the continuous space to avoid unphysical flow effects, and a sufficient condition for lattice models to recover any of the macroscopic equations is high symmetry and the isotropy of lattice tensors. This is the main reason employing the multi-speed square lattice in our LBM simulation. Other lattices of different shapes may be used as long as they do not bring along the problems mentioned above, and their applications are straightforward. Figure 1 shows the square lattice employed in this work; the lattice vectors consist merely of unity components, which specify the propagation directions of particles after local collisions. Discretising the discrete Boltzmann equation in 2D yields

$$\frac{F_i\left(\hat{x},\hat{y},\hat{t}+\Delta\hat{t}\right)-F_i\left(\hat{x},\hat{y},\hat{t}\right)}{\Delta\hat{t}}+c_{ix}\frac{F_i\left(\hat{x}+\Delta\hat{x},\hat{y},\hat{t}+\Delta\hat{t}\right)-F_i\left(\hat{x},\hat{y},\hat{t}+\Delta\hat{t}\right)}{\Delta\hat{x}}$$
$$+c_{iy}\frac{F_i\left(\hat{x},\hat{y}+\Delta\hat{y},\hat{t}+\Delta\hat{t}\right)-F_i\left(\hat{x},\hat{y},\hat{t}+\Delta\hat{t}+\Delta\hat{t}\right)}{\Delta\hat{y}}=-\frac{1}{\hat{t}e}\left[F_i\left(\hat{x},\hat{y},\hat{t}\right)-F_i^{eq}\left(\hat{x},\hat{y},\hat{t}\right)\right] \quad (8)$$

Substituting $\Delta\hat{x}/\Delta\hat{t}=\Delta\hat{y}/\Delta\hat{t}=|c_i|=c$, equation (8) has the final form of:

$$\frac{F_i\left(\hat{\vec{x}},\hat{t}+\Delta\hat{t}\right)-F_i\left(\hat{\vec{x}},\hat{t}\right)}{\Delta\hat{t}}+\frac{F_i\left(\hat{\vec{x}}+c_i\Delta\hat{t},\hat{t}+\Delta\hat{t}\right)-F_i\left(\hat{\vec{x}},\hat{t}+\Delta\hat{t}\right)}{\Delta\hat{t}}$$
$$=-\frac{1}{\hat{t}e}\left[F_i\left(\hat{\vec{x}},\hat{t}\right)-F_i^{eq}\left(\hat{\vec{x}},\hat{t}\right)\right] \quad (9)$$

$$\frac{F_i\left(\hat{\vec{x}}+c_i\Delta\hat{t},\hat{t}+\Delta\hat{t}\right)-F_i\left(\hat{\vec{x}},\hat{t}\right)}{\Delta\hat{t}}=-\frac{1}{\hat{t}e}\left[F_i\left(\hat{\vec{x}},\hat{t}\right)-F_i^{eq}\left(\hat{\vec{x}},\hat{t}\right)\right] \quad (10)$$

We hence obtain the discretized discrete Boltzmann equation in lattice Boltzmann context; by further restricting the spatial and temporal dimension to be of molecular order, i.e. $\frac{\Delta\hat{x}}{l}\approx O\left(\frac{\Delta\hat{t}}{t}\right)$, we obtain the lattice velocity in terms of the mean free path l and the relaxation time t:

$$\frac{\Delta\hat{x}}{\Delta\hat{t}}=\frac{l}{t}=c_i \quad (11)$$

This lattice velocity $c_i=\left(c_{ix},c_{iy}\right)$, to be of unity magnitudes for direction *i = 1, 3, 5,* and *7*, and of magnitude $\sqrt{2}$ for directions *i = 2, 4, 6* and *8* otherwise, has its velocity components in *x* and *y* directions shown in Figure 1.

To start the simulation, the desired *Kn* (λ/H) was first chosen. In defining *Kn* in lattice context, we wrote λ and *H* in terms of $\tau, \Delta x, \Delta t$ and number of mesh in Y direction in their physical dimensions:

$$\lambda = \tau \frac{\Delta x}{\Delta t}, \qquad H = \Delta y N_y \tag{12}$$

$$Kn = \frac{\tau \left(\Delta x / \Delta t \right)}{\Delta y N_y} = \frac{\hat{\tau}}{N_y}, \quad or \qquad \tau = Kn N_y \tag{13}$$

where τ in equation (13) represents the dimensionless relaxation without the caret. Having defined *Kn*, appropriate N_y *and* τ could then be selected, which would then be used in the determination of mesh size and the collision-propagation updating procedure respectively. Note that the degree of rarefaction is affected by 2 factors, namely the mean free path (density) and the characteristic length. Although there is no proof in equating same degree of rarefaction by low density (large λ) and by minute geometries (small *L*), we treat this dimensionless number *Kn* here as general, irrespective of its origin. With this approach, there is literally no restriction on the flow regime from the point of governing equations, as encountered by its N-S solvers counterpart, in which rarefaction breaks down the continuum of flow and cause N-S approach to be invalid at high *Kn.*

It is worth noting that the lattice velocity definition which requires Δx and Δt to be of the same order of λ and τ respectively automatically satisfies our intrinsic criterion

for micro flow that the particles' interactions are restricted to collisional time and space in microscopic level. Particles are assumed to travel a distance of $\boldsymbol{l}$ while relaxing to their equilibrium state in duration $\boldsymbol{t}$. Hence, the overall collision time t_c is very similar, and in our assumption equal to the relaxation time $\boldsymbol{t}$. Note also that parameter $\boldsymbol{e}$ in Equation (10) marks the rarefaction effect in the governing equation when used in rarefaction context. The role of $\boldsymbol{e}$, which is analogous to *Kn* as discussed earlier is practically the same as that of *Re* in Navier-Stokes equations. Choosing $\Delta t = t_c$ and dropping the carets leads to the conventional Lattice Boltzmann BGK equation:

$$F_i\left(\vec{x} + c_i\Delta t, t + \Delta t\right) - F_i\left(\vec{x}, t\right) = -\frac{1}{\boldsymbol{t}}\left[F_i\left(\vec{x}, t\right) - F_i^{eq}\left(\vec{x}, t\right)\right] \tag{14}$$

Up to this point, we are still on the same basis that conventional LBM stands, therefore the definitions of the density distribution, momentum and pressure still apply:

$$\boldsymbol{r} = \sum_{i=0}^{k} F_i, \qquad \boldsymbol{r}U = \sum_{i=1}^{k} c_i F_i, \qquad P = \frac{1}{3}\boldsymbol{r}c^2 \tag{15}$$

As such, the equilibrium distribution functions approximated from a Maxwellian distribution [11,14] can be defined as:

$$F_0^{eq} = \frac{4}{9}\rho\left[1 - \frac{3}{2}\frac{U^2}{c^2}\right] \tag{16}$$

$$F_i^{eq} = \frac{1}{9}\rho\left[1 + 3\frac{c_i \cdot U}{c^2} + \frac{9}{2}\frac{(c_i \cdot U)^2}{c^4} - \frac{3}{2}\frac{U^2}{c^2}\right] \qquad i = 1, 3, 5, 7 \tag{17}$$

$$F_i^{eq} = \frac{1}{36}\rho\left[1 + 3\frac{c_i \cdot U}{c^2} + \frac{9}{2}\frac{(c_i \cdot U)^2}{c^4} - \frac{3}{2}\frac{U^2}{c^2}\right] \qquad i = 2, 4, 6, 8 \tag{18}$$

In the traditional approach, while recovering Navier-Stokes equations in macroscopic limit through a multi-scale (Chapman-Enskog) expansion technique, the flow parameter such as the kinematic viscosity ν can be defined [15], which will then be used in constructing the Reynolds number. As will be shown in the next section, we discuss a different flow parameter necessary to be looked into as stated in discrete Boltzmann equation (6), where the Knudsen number instead of the Reynolds number is present and becomes the main flow parameter in addition to the density distribution functions.

b. Flow simulation by Lattice Boltzmann Method

The channel was assumed to have linear pressure distribution and the fluid in the channel at rest initially. As the flow was pressure driven, the flow boundary ($i = 1$, and $i = imax$) pressures were fixed at constant ratio at every time step, from which the undetermined density distribution functions could be approximated by their equilibrium distribution functions, whose u and v velocities were extrapolated from the flow domain accordingly. Figure 2 shows lattice nodes with their 3 unknown functions (dashed lines)

in the flow boundaries. As mentioned earlier, the pre-fixed values of pressure (and hence density) together with the extrapolated u and v velocities defined the 3 unknown functions at flow boundaries, as follows:

$$\left.\begin{aligned} F_1(x,y,t) &= F_1^{eq}(\rho,u,v,x,y,t) \\ F_2(x,y,t) &= F_2^{eq}(\rho,u,v,x,y,t) \\ F_8(x,y,t) &= F_8^{eq}(\rho,u,v,x,y,t) \end{aligned}\right\} \text{at inlet} \tag{19}$$

$$\left.\begin{aligned} F_5(x,y,t) &= F_5^{eq}(\rho,u,v,x,y,t) \\ F_4(x,y,t) &= F_4^{eq}(\rho,u,v,x,y,t) \\ F_6(x,y,t) &= F_6^{eq}(\rho,u,v,x,y,t) \end{aligned}\right\} \text{at outlet} \tag{20}$$

On the solid boundaries ($j = 1$, and $j = jmax$), we incorporated specular bounce back to have 3 unknown distribution functions (Figure 3) defined, as follows:

$$\left.\begin{aligned} F_2(x,y,t) &= F_8(x,y,t) \\ F_3(x,y,t) &= F_7(x,y,t) \\ F_4(x,y,t) &= F_6(x,y,t) \end{aligned}\right\} \text{at lower wall} \tag{21}$$

$$\left.\begin{aligned} F_8(x,y,t) &= F_2(x,y,t) \\ F_7(x,y,t) &= F_3(x,y,t) \\ F_6(x,y,t) &= F_4(x,y,t) \end{aligned}\right\} \text{at upper wall} \tag{22}$$

This is analogous to a reflection of a particle hitting a wall specularly, taking the distribution function as a representation of a group of particles having the same velocity approaching the wall. Earlier bounce back scheme [16] was used heuristically to ensure no slip condition while this specular scheme enables us to capture the slip at wall.

In addition to specular bounce back, we introduce an extrapolation scheme which approximates the flow variables at solid boundaries by a 2nd order polynomial extrapolation scheme. The unknown functions at wall are then approximated to their equilibrium functions, which are sufficiently made up of the extrapolated flow variables:

$$\boldsymbol{j}(x,y,t) = 3\boldsymbol{j}(x,y\pm 1,t) - 3\boldsymbol{j}(x,y\pm 1,t) + \boldsymbol{j}(x,y\pm 1,t) \tag{23}$$

$$F_i^W(x,y,t) = F_i^{eq}(\boldsymbol{j},x,y,t) \tag{24}$$

where F_i^W is the unknown distribution function at wall boundary in Figure 2 and $\boldsymbol{j}$ represents flow variables $\boldsymbol{r}$, and u. This approximation may be justified by the fact that all distribution functions eventually converge to their equilibrium states. The main objective here is to investigate the direct effects of boundary treatments used in the lattice boundaries on the entire flow properties, and more importantly, their contributions to slip velocities.

Since Equation (14) mainly describes the particle activities in the simulated flow, i.e. local collision and propagation, it can be split into 2 numerical steps accordingly:

$$F_i^*(\vec{x},t) = F_i(\vec{x},t) - \frac{1}{\boldsymbol{t}}\left[F_i(\vec{x},t) - F_i^{eq}(\vec{x},t)\right] \tag{25}$$

$$F_i(\vec{x} + c_i\Delta t, t+\Delta t) = F_i^*(\vec{x},t) \tag{26}$$

Upon calculating all F^{eq}'s which are only functions of the macroscopic parameters (namely ρ, u, and v) in the flow domain, local collisions will be performed (Equation (25)), which is followed by global propagations (Equation (26)). Those distribution functions at boundaries that cannot be determined by propagation procedure are exceptional to this algorithm and will be attained according to our boundary treatments mentioned earlier.

III. Results and Discussions

Beskok et al [17] proposed that there were 4 major effects occur in micro flow, namely rarefaction, compressibility, thermal creeping and viscous heating. The first 2 effects will be more relevant in our present isothermal analyses, which can be shown by our pressure and velocity analyses. We are particularly interested in the Slip Flow regime ($0.01 < Kn < 0.1$) where the flow is still deemed valid when solved using Navier-Stokes equations with slip boundary condition. 4 cases were simulated, i.e. 2 dimensional micro-channel flow with $Kn = 0.05$ and 0.1 with 2 boundary treatments mentioned earlier, i.e. specular bounce back (*Spec*) and the extrapolation method (*U Ext*.). Arkilic et al [18] obtained analytical Navier-Stokes solution at low *Re* and *Ma* with a first order slip model for 2D micro-channel flow, in which the general pressure and velocity profiles were described. In Figures 3-5, our numerical results yield the same profiles as given by Arkilic et al, and these profiles remain similar in general in our present numerical simulations. In this section, the negation of non-linearity in pressure distribution (compressibility) as *Kn* increases is discussed, and experimental results from UCLA [19]

are also benchmarked to examine our numerical results in Transition Flow regime ($0.1 < Kn < 3$). In spite of the differences in modelling approaches, both Arkilic and present results are expected to be comparatively similar since both of them fall within the same Slip Flow regime, as illustrated in Figures 6-12.

Figure 3 shows the pressure distribution in the channel, where the pressure P^* has been normalized by the outlet pressure, and the x-coordinate to the channel length. * here denotes the non-dimensionalisation of a flow variable. It can be shown that P^* is only dependent on X, and that it remains unchanged across the channel. Figures 4 and 5 illustrate the u and v velocities respectively. In general, Figure 4 exhibits the general characteristics of micro-channel flow, in which the slip and centreline velocities increase along the channel due to decreasing pressure, and that the parabolic velocity profile across the channel is symmetrical throughout. Figure 5 confirms the v profile obtained by Arkilic et al [18], in which the velocity is zero at the centreline and solid boundaries, and that the maximum points are opposite to each other and skewed towards the walls. However, its relative importance is not as significant as P^* and u, because its magnitude is of several order smaller. Nonetheless, this characteristic of flow captured by the present approach confirms the existence of lateral velocity v as shown in the analytical solution.

In Figure 6, we compare the non-linearity of pressure $\left(P' = P_x^* - P_{linear}^*\right)$ obtained by various methods mentioned earlier at $Pr = 2.0$ within Slip Flow regime, at $Kn = 0.05$ and $Kn = 0.10$ respectively. Similar to that predicted by the analytical solutions, both

boundary treatment schemes are able to show the negation of non-linearity in pressure $\left(P' = P_x^* - P_{linear}^*\right)$ as rarefaction increases. This non-linearity in pressure distribution is a consequence of the compressibility effect in micro flow according to Beskok et al. Figures 7 and 8 on the other hand illustrate P' for a spectrum of pressure ratios ranging $2.0 < Pr < 3.0$ obtained using different boundary treatment schemes. The compressibility effect is enhanced by larger pressure ratios in both cases, and there is also a consistent deficit in magnitude between our numerical results and Arkilic's, which are more obviously illustrated in Figures 9 and 10. This may be the case since the rarefaction effect is only accounted for in Arkilic's solution by incorporating a first order slip while we look at the issue in a more rarefied sense where the molecular dimensions are concerned. In concluding this remark, we compare both present results and Arkilic's results to *UCLA* experimental results [19], as shown in Figures 9 and 10: Arkilic's results over-predict P' in both cases, and the over-prediction becomes more obvious at larger *Kn*. Our results show that the non-linearity in pressure which is reverse indicator of rarefaction does not vary much for both boundary schemes. This suggests that the boundary treatment mechanism has little influence on the pressure distribution. Another interesting point is that the peak of non-linearity is skewed towards the outlet; this phenomenon is clearly exhibited by both Arkilic's and present results. However, we report a more severe skewness, in which the peak occurs at $0.6 < X < 0.7$, compared to almost consistently at roughly *0.6* in Arkilic's results. It is also shown that larger pressure ratio will further delay the peak towards outlet and that *Kn* has little effect on its location. The effect of *Kn* is not fully realised, neither in Arkilic's nor in present results.

Figures 11 and 12 show the slip velocities along the channel that are normalised to the outlet centreline velocity predicted by Specular and Extrapolation schemes respectively. Both present results predict smaller slip on wall towards the outlet, with Specular model (Figures 11a and 11b) comparatively well fitted in the capsule of analytical predictions. Both models exhibit better resemblance at higher *Kn*, as depicted in Figures 11b and 12b. There are 2 features that are commonly shared: the decreasing trend for upstream slip at pressure rise and the convergence of a unique value of slip at outlet for various *Pr*'s. According to Arkilic et al [18], the slip at wall u_s^* at outlet is only dependent on *Kn*, given by Equation (27):

$$u_{s,o}^* = 1 - \frac{1}{1 + 4sKn_o} \tag{27}$$

where s is a parameter (accommodation factor) in Arkilic's solution and is set to 1, and Kn_o is the outlet Knudsen number. Since local Knudsen number is a function of density that varies along the channel, the outlet Knudsen number which is usually at atmospheric conditions and constant is used in representing the flow for general cases. In present work, we keep up this consistency and characterise every simulation case by their outlet Knudsen numbers. In general, slip at wall can be expressed in terms of outlet slip $u_{s,o}^*$ that is function of *Kn*, *Pr* and $\left.\frac{\partial P^*}{\partial X}\right|_x$, shown below:

$$u_s^* = \frac{\Theta}{Pr} U_{s,o}^* = \Psi u_{s,o}^* \tag{28}$$

where Θ denotes the ratio of local to outlet pressure gradient and the subscript *x* and *o* denote location along the channel and the outlet position respectively, in which case

$$\Theta = \frac{\partial P^* / \partial X\big|_x}{\partial P^* / \partial X\big|_o} \tag{29}$$

$$\left.\frac{\partial P^*}{\partial X}\right|_x = \frac{1 + 12\sigma Kn - \left(\mathrm{Pr}^2 + 12\sigma Kn \mathrm{Pr}\right)}{2\sqrt{(6\sigma Kn)^2 + (1 + 12\sigma Kn)x + \left(P^2 + 12\sigma Kn \mathrm{Pr}\right)(1 - x)}} \tag{30}$$

Parameter Ψ is inversely proportional to *Pr*; this explains Figures 11 and 12 about the reducing normalised inlet slip velocities. In general, slip velocity grows with *Pr*, but since the normalising parameter U_{max} grows more effectively than u_s, we observe a decline in slip as *Pr* increases. Both of our boundary schemes predict the outlet slip (*Pr* invariant) to be generally lower than that by N-S first order slip model. The reasoning of this may be that mere first order slip incorporation in N-S equations does not sufficiently and accurately account for the slip phenomenon. Also N-S equations, which is macroscopic in nature, does not account for rarefaction effect intrinsically, and this in turn over-predict the compressibility (non-linearity) as well as slip as external first order approximation has to be used to make the flow 'rarefied'.

IV. Concluding Remarks

Here we present a particle-based LBM scheme in solving discrete Boltzmann equation, whose validity is more appropriately justified for micro flow. We look at a simple 2D pressure driven channel flow paying particular attention to the pressure distribution and the slip velocity along the channel. Next, we validate our scheme in Slip Flow and Transition Flow regimes, comparing the numerical results with experimental data as well as analytical solution based on N-S equations. Finally, the immediate effects of *Kn* and *Pr* on non-linearity of pressure and slip are also discussed briefly. Our numerical results confirm the rarefaction's negation on non-linearity of pressure, that the normalised slip diminishes with *Pr*, and that the normalised outlet slip is only dependent on *Kn* but not *Pr*. The slip predicted by both boundary schemes here fall in the spectrum of that predicted by analytical solution, particularly at higher *Kn* in Slip flow regime. In the present work, we only look at micro flow in rarefaction context, in doing so, we have disregarded particles' molecular constitution and overlooked the possible rarefaction disparities due to low density and miniature dimension.

References

[1] Bird, G. A., 1994, "Molecular Gas Dynamics and the Direct Simulation of Gas Flows," ISBN 0198561954, Oxford University Press, New York.

[2] Higuera, F. J. and Jimenez, J., 1989, "Boltzmann Approach to Lattice Gas Simulations," *Europhysics Letter*, Vol. 9, No. 7, pp. 663-668.

[3] Abe, T., 1997, "Derivation of the lattice Boltzmann Method by Means of the Discrete Ordinate Method for the Boltzmann Equation," *journal of Computational Physics*, Vol. 131, pp. 241-246.

[4] He, X. and Luo, L.-S., 1997, "A Priori Derivation of the Lattice Boltzmann Equation," *Physical Review E*, Vol. 55, pp. 6333-6336.

[5] McNamara, G. R. and Zanetti, G., 1988, "Use of the Boltzmann Equation to Simulate Lattice-Gas Automata," *Physical Review Letter*, Vol. 61, No. 20, pp. 2332-2335.

[6] Frisch, U., Hasslacher, B., Pomeau, Y., 1986, "Lattice-Gas Automata for the Navier-Stokes Equation," *Physical Review Letter*, Vol. 56, No. 14, pp. 1505-1508.

[7] Chen, S., Chen H. D., Martinez, D., and Matthaeus, W. H., 1991, "Lattice Boltzmann Model for Simulation of Magnetohydrodynamics," *Physical Review Letter*, Vol. 67, pp. 3776-3779.

[8] Qian, Y. H., 1990, "Lattice Gas and Lattice Kinetic Theory Applied to the Navier-Stokes equation," *PhD Thesis*, Université Pierre et Marie Cure, Paris.

[9] Bhatnagar, P. L., Gross, E. P., and Krook, M., 1954, "A Model for Collision Processes in Gases. I. Small Amplitude Processes in Charged and Neutral One-Component Systems," *Physical Review*, Vol. 94, No. 3, pp. 511-525.

[10] Wolf-Gladrow, D. A., 2000, "Latice-Gas Cellular Automata and Lattice Boltzmann Models: An Introduction," *Lecture Notes in Mathematics 1725*, Springer-Verlag, Germany, ISBN 3-540-66973-6, pp. 174-182.

[11] Qian, Y. H., d'Humières, D., and Lallemand, P., 1992, "Lattice BGK Models for Navier-Stokes Equation," *Europhysics Letter*, Vol. 17, No. 6, pp. 479-484.

[12] Gunstensen, A. K. and Rothman, D. H., 1991, "A Galilean-Invariant Immiscible Lattice Gas," *Physica D*, Vol. 47, pp. 53-63.

[13] Chen, Y., Lee, M., Zhao, K. H., and Doolen, G. D., 1989, "A Lattice Gas Model with Temperature," *Physica D*, Vol. 37, pp. 42-59.

[14] Chen, H., Chen, S., and Matthaeus, W. H., 1992, "Recovery of the Navier-Stokes Equations Using a Lattice-Gas Boltzmann Method," *Physical Review A*, Vol. 45, No. 8, pp. R5339-R5342.

[15] He, X. Zou, Q., Luo, L.-S., and Dembo, M., 1997, "Analytic Solutions of Simple Flows and Analysis of Nonslip Boundary Conditions for the Lattice Boltzmann BGK Model," *Journal of Statistical Physics*, Vol. 87, No. 1 / 2, pp. 115-136.

[16] Ziegler, D. P., 1993, "Boundary Conditions for Lattice Boltzmann Simulations," *Journal of Statistical Physics*, Vol. 71, No. 5 / 6, pp. 1171-1177.

[17] Beskok, A., Karniadakis, G. E., and Trimmer, W., 1996, "Rarefaction and Compressibility Effects in Gas Microflows," *Journal of Fluids Engineering*, Vol. 118, pp. 448-456.

[18] Arkilic, E. B., Schmidt, M. A., and Breuer, K. S., 1997, "Gaseous Slip Flow in Long Microchannels," *Journal of Microelectromechanical Systems*, Vol. 6, No. 2, pp. 167-178.

[19] Huang, J., 1998, "Thermal Lattice BGK Models for Fluid Dynamics," *PhD Thesis*, Drexel University, pp. 58-68.

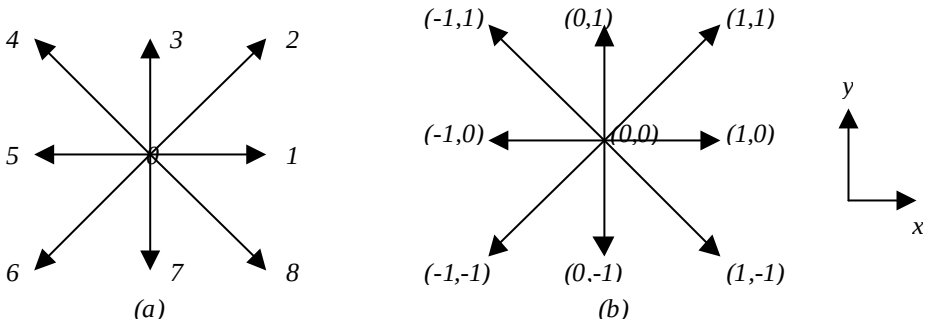

Fig. 1 A D2Q9 Lattice Model: (a) lattice Directions; (b) Lattice Velocity Vectors

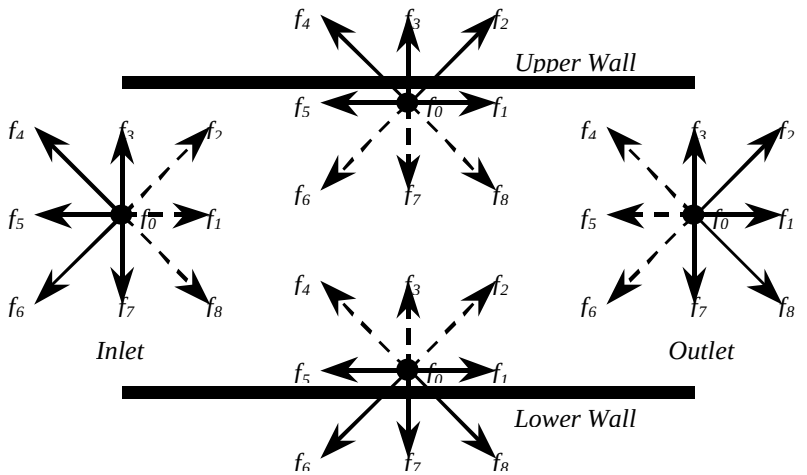

Fig. 2 Configuration of Distribution Functions at Boundary Points

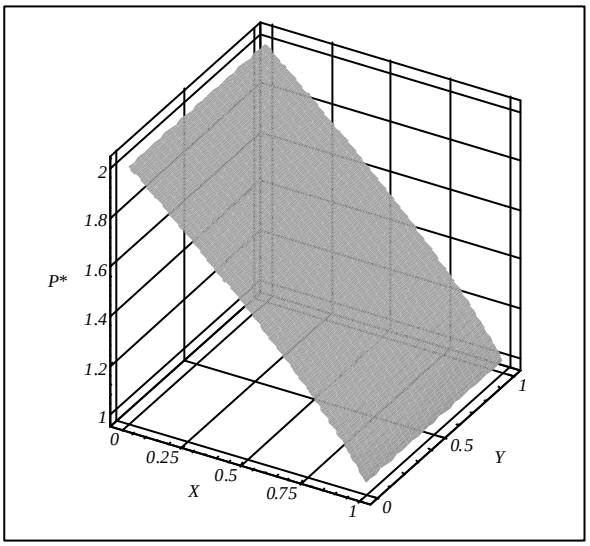

Fig. 3 Normalised Pressure Distributions Predicted by Specular Scheme

at *Pr = 2.00, Kn = 0.05*

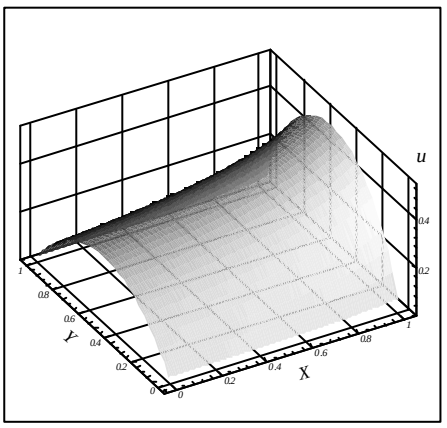

Fig. 4 *u*-Velocity Profile Predicted by Specular Scheme at *Pr = 2.00, Kn = 0.05*

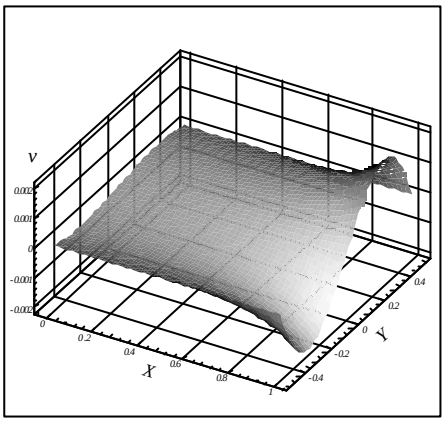

Fig. 5 *v*-Velocity Profile Predicted by Specular Scheme at *Pr = 2.00, Kn = 0.05*

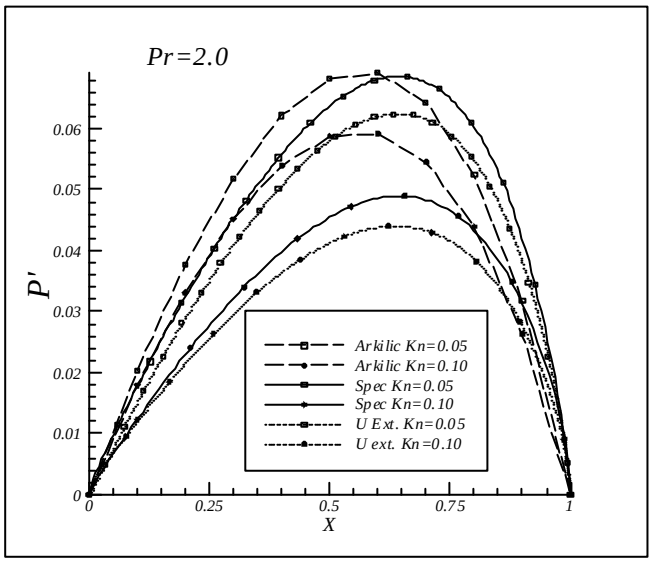

Fig. 6 Comparison of Non-linearity of Pressure P' Obtained by Specular (Spec) and Extrapolation (U Ext.) Schemes with Analytical Solution at Pr=*2.0*, Kn=*0.05, 0.1*

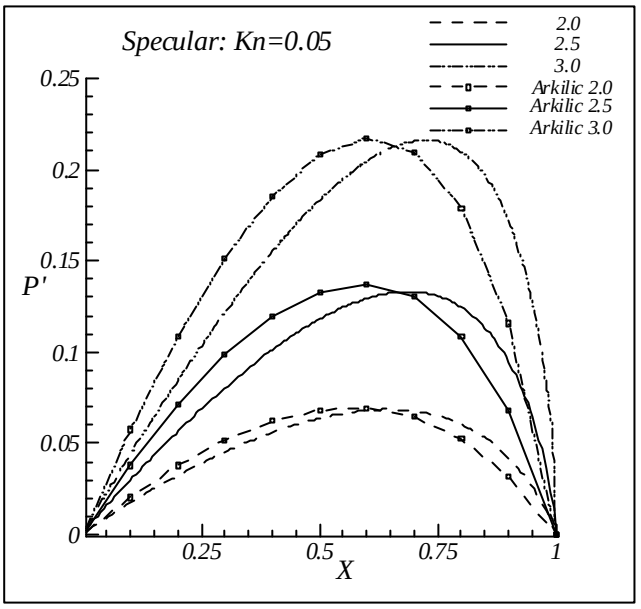

(a) Results of *Kn*=0.05

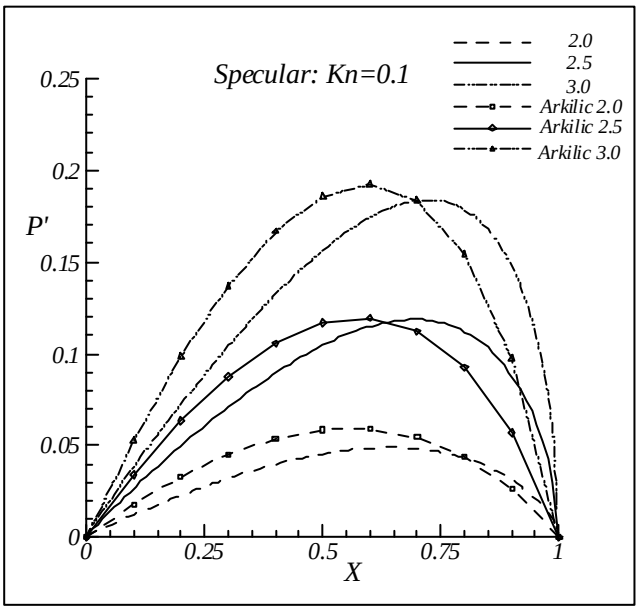

(b) Results of *Kn*=0.1

Fig. 7 Comparison of Non-linearity of Pressure P' Obtained by Specular (Spec) Scheme with Analytical Solution at *Kn*=0.05, 0.1 and Different Pressure Ratios

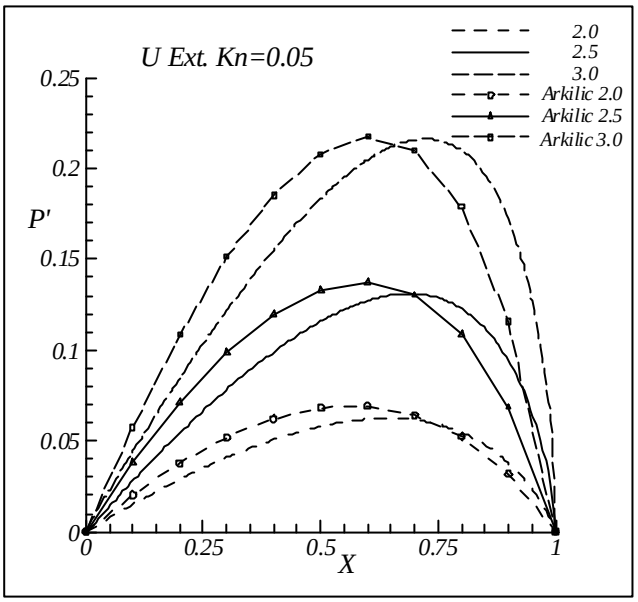

(a) Results of *Kn*=0.05

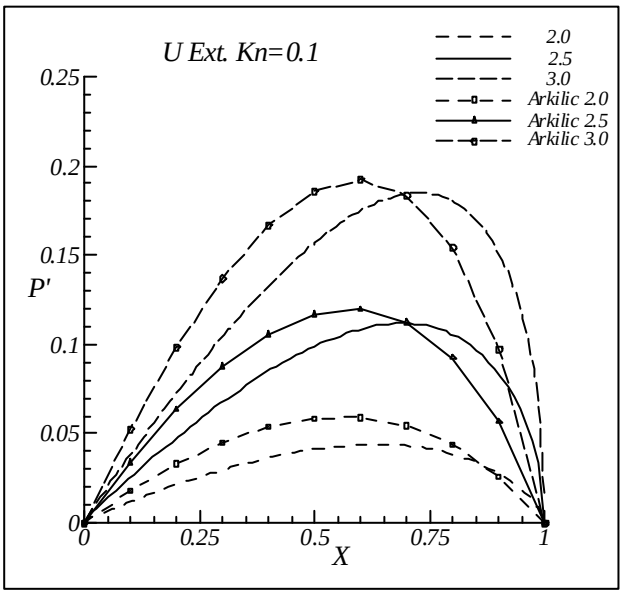

(b) Results of *Kn*=0.1

Fig. 8 Comparison of Non-linearity of Pressure P' Obtained by Extrapolation (U ext) Scheme with Analytical Solution at *Kn*=0.05, 0.1 and Different Pressure Ratios

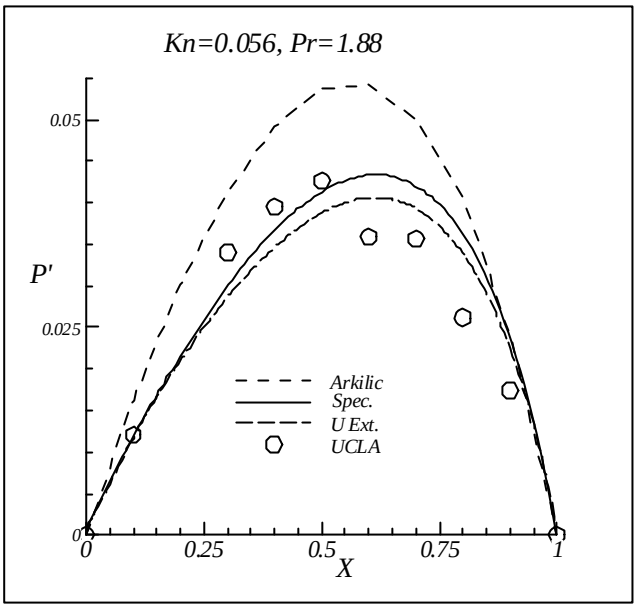

Fig. 9 Comparison of Non-linearity of Pressure P' Between Present Results, Arkilic's Analytical Results and Experimental Data at *Pr*=1.88, *Kn*=0.056

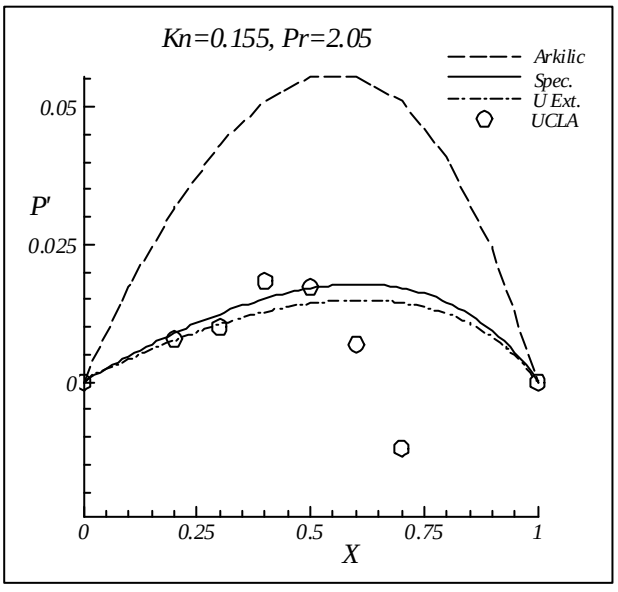

Fig. 10 Comparison of Non-linearity of Pressure P' Between Present Results, Arkilic's Analytical Results and Experimental Data at *Pr*=2.05, *Kn*=0.155

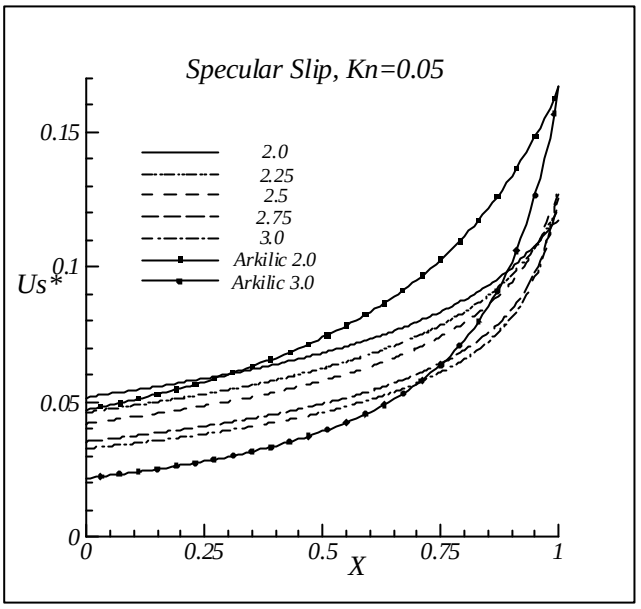

(a) Results of *Kn*=0.05

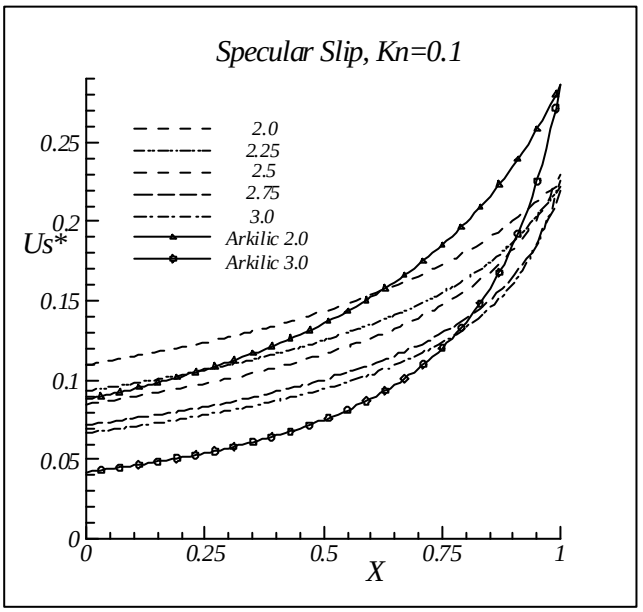

(b) Results of *Kn*=0.1

Fig. 11 Comparison of Slip Velocity at Wall between Present Results Obtained by Specular (Spec) Scheme and Arkilic's Analytical Results at *Kn*=0.05, 0.1 and Different Pressure Ratios

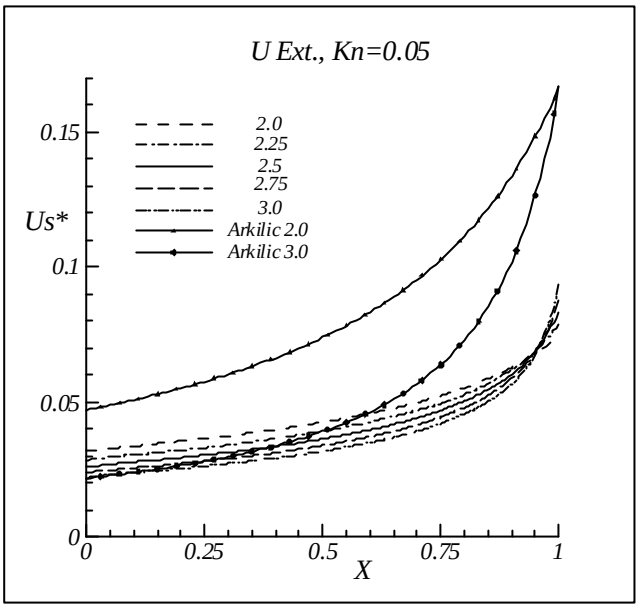

(a) Results of *Kn*=0.05

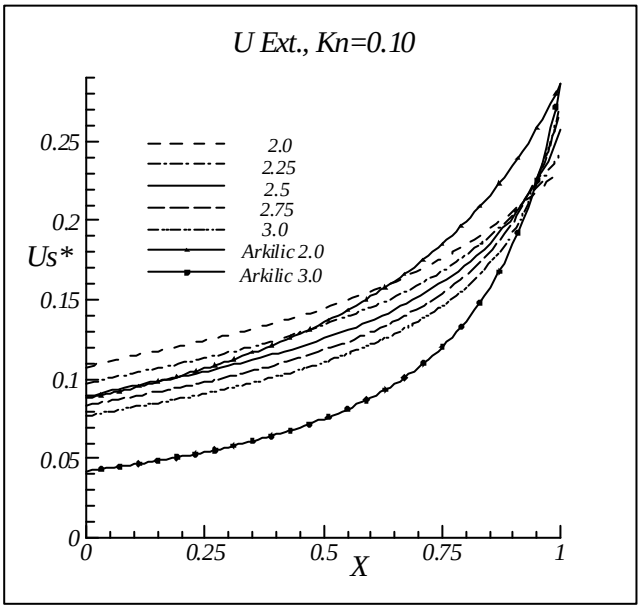

(b) Results of *Kn*=0.1

Fig. 12 Comparison of Slip Velocity at Wall between Present Results Obtained by Extrapolation (U ext) Scheme and Arkilic's Analytical Results at *Kn*=0.05, 0.1 and Different Pressure Ratios